Arch Appl Mech (2014) 84:571–590
DOI 10.1007/s00419-014-0818-1

ORIGINAL

Rajneesh Kumar · Mandeep Kaur

Reflection and refraction of plane waves at the interface of an elastic solid and microstretch thermoelastic solid with microtemperatures

Received: 16 March 2013 / Accepted: 10 January 2014 / Published online: 7 February 2014
© Springer-Verlag Berlin Heidelberg 2014

Abstract The problem of reflection and refraction of waves at the interface of an elastic solid and microstretch thermoelastic solid with microtemperatures has been investigated. It is shown that due to incidence of P-wave or SV-wave at the interface, the waves are reflected and refracted. The amplitude ratios of these various reflected and refracted waves have been computed numerically, and graphical representation of their variations is made with the angle of incidence. Effect of microrotation on these amplitude ratios has been shown graphically. Some particular cases of interest have also been discussed.

Keywords Elastic solid · Microstretch · Microtemperatures · Reflection and refraction · Amplitude ratios

1 Introduction

It is known that material response to external stimuli is dependent heavily on the motions of its inner structures. Classical elasticity ignores this effect by ascribing only translation degrees of freedom to material points of body. Eringen [1] developed the micropolar theory by including intrinsic rotations of the microstructure which can support body and surface couples and display high-frequency optical branch of the wave spectrum. For engineering applications, it can model composites with rigid chopped fibers, elastic solids with rigid granular inclusions, and other industrial materials such as liquid crystals Eringen [2–4].

The theory of microstretch elastic bodies developed by Eringen [5] is a generalization of the micropolar theory. Eringen [6] also developed the theory of thermo-microstretch elastic solids. Microstretch continuum represents a model for Bravais lattice with basis on the atomic level and two phase dipolar solid with a core on the macroscopic level. Composite materials reinforced with chopped elastic fibers, porous media whose pores are filled with gas or inviscid liquid, asphalt, or other elastic inclusions and "solid-liquid" crystals, etc. should be characterizable by microstretch solids. This model is a generalization of the micropolar theory and a special case of the micromorphic theory Eringen [7,8], which Eringen introduced several decades back.

Micropolar theory is now well established, and it has found many important applications, while the mathematical challenges presented by micromorphic theory make it dormant. Microstretch theory is much simpler, still it does not possess the scope of physical phenomena covered by the micromorphic continuum mechanics and can be used as a mathematical model for many different material media that fall outside the domain of micropolar elasticity.

R. Kumar
Department of Mathematics, Kurukshetra University, Kurukshetra 136119, India
E-mail: rajneesh_kuk@rediffmail.com

M. Kaur (✉)
Department of Applied Sciences, Guru Nanak Dev Engineering College,
Ludhiana 141008, Punjab, India
Tel: +91-946-3055900
E-mail: mandeep1125@yahoo.com

Singh [9] studied reflection of plane waves from free surface of a microstretch elastic solid, Singh and Kumar [10] discussed wave propagation in a generalized thermo-microstretch elastic solid, Ciarletta and Scalia [11] give some result in linear theory of thermo-microstretch elastic solids, Iesan and Quintanilla [12] studied thermal stresses in microstretch elastic plates, and Tomar and Khurana [13] discussed reflection and transmission of elastic waves from a plane interface between two thermo-microstretch solid half-spaces. Various authors studied problems in thermo-microstretch medium, e.g., [14–29].

Grot [30] settled a theory of thermodynamics of elastic bodies with microstructure whose microelements possess microtemperatures. The Clausius–Duhem inequality is improved to include microtemperatures, and the first-order moment of the energy equations are added to the usual balance laws of a continuum with microstructure.

Riha [31] studied heat conduction in materials with microtemperatures. Experimental results for the silicone rubber containing spherical aluminum particles and for human blood were found to conform closely to predicted theoretical thermal conductivity. The linear theory of thermoelasticity with microtemperatures for materials with inner structure whose particles, in addition to the classical displacement and temperature fields, possess microtemperatures was presented by Iesan and Quintanilla [32].

Iesan [33] proposed the theory of micromorphic elastic solids with microtemperatures. Various problems using thermoelasticity with microtemperatures were studied by Iesan and Quintanilla [34]. Exponential stability in thermoelasticity with microtemperatures was studied by Casas and Quintanilla [35]. Scalia and Svandze [36] give the representation of solutions of the theory of thermoelasticity with microtemperatures and Iesan [37] discussed thermoelasticity of bodies with microstructure and microtemperatures. Aouadi [38] studied some theorems in the isotropic theory of microstretch thermoelasticity with microtemperatures. Scalia et al. [39] studied basic theorems in the equilibrium theory of thermoelasticity with microtemperatures. Quintanilla [40] discussed the growth and continuos dependence in thermoelasticity with microtemperatures, Steeb et al. [41] studied time harmonic waves in thermoelastic material with microtemperatures. Chirita et al. [42] studied the theory of thermoelasticity with microtemperatures.

The purpose of the present paper is to analyze the reflection and refraction of waves at the boundary between an elastic half-space and microstretch thermoelastic half-space with microtemperatures. The amplitude ratios of reflected longitudinal wave (P-wave), transverse wave (SV-wave) and refracted longitudinal displacement wave (LD-wave), thermal wave (T-wave), microstretch wave (LM-wave), microtemperature wave (LT-wave), transverse displacement wave coupled with microrotational wave, and microtemperature wave (namely CD-I wave, CD-II wave and CD-III wave) have been obtained and presented graphically as a function of angle of incidence. The microrotational effect on these amplitude ratios is shown for a particular model.

2 Basic equations

Following Eringen [6] and Iesan [43], the field equations and constitutive relations for a homogeneous, isotropic microstretch thermoelastic solid with microtemperatures without body forces, body couples, stretch force, heat sources, and first heat source moment are

(i) Stress equation of motion:

$$(\lambda + 2\mu + K)\nabla(\nabla.\boldsymbol{u}) - (\mu + K)\nabla \times (\nabla \times \boldsymbol{u}) + K(\nabla \times \boldsymbol{\varphi}) + \lambda_0 \nabla\phi^* - \nu\nabla T = \rho \frac{\partial^2 \boldsymbol{u}}{\partial t^2}, \tag{1}$$

(ii) Couple stress equation of motion:

$$(\alpha + \beta + \gamma)\nabla(\nabla.\boldsymbol{\varphi}) - \gamma\nabla \times (\nabla \times \boldsymbol{\varphi}) + K(\nabla \times \boldsymbol{u}) - 2K\boldsymbol{\varphi} - \mu_1(\nabla \times \boldsymbol{w}) = \rho j \frac{\partial^2 \boldsymbol{\varphi}}{\partial t^2}, \tag{2}$$

(iii) Equation of balance of stress moments:

$$\alpha_0 \nabla^2 \phi^* + \nu_1 T - \lambda_1 \phi^* - \lambda_0 (\nabla.\boldsymbol{u}) - \mu_2(\nabla.\boldsymbol{w}) = \rho \frac{j_0}{2} \frac{\partial^2 \phi^*}{\partial t^2}, \tag{3}$$

(iv) Equation of balance of energy:

$$K^* \nabla^2 T - \rho c^* \frac{\partial T}{\partial t} - \nu_1 T_0 \frac{\partial \phi^*}{\partial t} - \nu T_0 (\nabla.\boldsymbol{u}) + k_1(\nabla.\boldsymbol{w}) = 0, \tag{4}$$

(v) Equation of balance of first moment of energy:

$$k_6\nabla^2\boldsymbol{w} + (k_4+k_5)\nabla(\nabla.\boldsymbol{w}) + \mu_1\frac{\partial}{\partial t}(\nabla\times\boldsymbol{\varphi}) - \mu_2\frac{\partial}{\partial t}(\nabla\phi^*) - b\frac{\partial \boldsymbol{w}}{\partial t} - k_2\boldsymbol{w} - k_3\nabla T = 0, \tag{5}$$

(vi) Constitutive relations:

$$t_{ij} = \lambda u_{r,r}\delta_{ij} + \mu\left(u_{i,j}+u_{j,i}\right) + K\left(u_{j,i} - \varepsilon_{ijr}\phi_r\right) - \nu T\,\delta_{ij} + \lambda_0\phi^*\delta_{ij}, \tag{6}$$

$$m_{ij} = \alpha\phi_{r,r}\delta_{ij} + \beta\phi_{i,j} + \gamma\phi_{j,i} + b_0\varepsilon_{mji}\phi^*_m, \tag{7}$$

$$\lambda^*_i = \alpha_0\phi^*_{,i} + b_0\varepsilon_{ijm}\phi_{j,m}, \tag{8}$$

$$q_{ij} = -k_4 w_{r,r}\delta_{ij} - k_5 w_{i,j} - k_6 w_{j,i}, \quad i,j,m = 1,\ 2,\ 3 \tag{9}$$

In the above $K,\ \alpha,\ \beta,\ \gamma,\ \lambda,\ \mu, \alpha_0, \lambda_0, \lambda_1, \mu_1, \mu_2, j_0, k_i (i = 1, \ldots\ldots\ldots\ldots, 6)$ are constitutive coefficients. The t_{ij} and m_{ij} are the components of stress tensor and couple stress tensor, λ^*_i is the microstress tensor, q_{ij} is the first heat flux moment tensor, $\boldsymbol{u}$ and $\boldsymbol{\varphi}$ are the displacement and microrotation vectors, $\boldsymbol{w}$ is the microtemperature vector and ϕ^* is the scalar microstretch, ρ is the density, j is the microinertia, $c^*$is the specific heat at constant strain, K^* is the thermal conductivity, T is the thermodynamic temperature, T_0 is the reference temperature,$\alpha_{T_1}, \alpha_{T_2}$ are the coefficients of linear thermal expansion.

Following Bullen [44], the equation of motion and constitutive relation of isotropic elastic solid

$$(\lambda^e+\mu^e)\nabla\left(\nabla.\boldsymbol{u}^e\right) + \mu^e\nabla^2\boldsymbol{u}^e = \rho^e\frac{\partial^2\boldsymbol{u}^e}{\partial t^2}, \tag{10}$$

$$t^e_{ij} = \lambda^e u^e_{r,r}\delta_{ij} + \mu^e\left(u^e_{i,j} + u^e_{j,i}\right), \tag{11}$$

where $\lambda^e,\ \mu^e$ are Lame's constants, $\boldsymbol{u}^e$ is the displacement vector, and ρ^e is density of an isotropic elastic solid.

3 Formulation of the problem and solution

An isotropic elastic solid half-space overlying a homogeneous isotropic, microstretch thermoelastic solid half-space with microtemperatures is considered. The origin of the Cartesian coordinate system $Ox_1x_2x_3$ is taken at any point on the plane surface (interface) and x_3-axis points vertically downwards into the microstretch thermoelastic solid half-space with microtemperatures. The region $x_3 \le 0$ is occupied by an elastic solid half-space (medium M_1), and microstretch thermoelastic solid half-space with microtemperatures occupies the region $x_3 \ge 0$ (medium M_2) as shown in Fig. 1. The plane waves are considered in the x_1x_3-plane with wave front parallel to the x_2-axis.

For two-dimensional problem, the displacement vector $\boldsymbol{u}$, microtemperature vector $\boldsymbol{w}$, microrotation vector $\boldsymbol{\varphi}$ in medium M_2, and displacement vector $\boldsymbol{u}^e$ in medium M_1 are thus taken as

$$\begin{aligned}&\boldsymbol{u} = (u_1(x_1,x_3),\ 0,\ u_3(x_1,x_3)), \qquad \boldsymbol{w} = (w_1(x_1,x_3),\ 0,\ w_3(x_1,x_3)), \qquad \boldsymbol{\varphi} = (0,\phi_2(x_1,x_3),0)\\ &\boldsymbol{u^e} = \left(u^e_1(x_1,x_3), 0, u^e_3(x_1,x_3)\right)\end{aligned} \tag{12}$$

The dimensionless quantities are

$$\begin{aligned}&x'_1 = \frac{x_1}{L} \quad x'_3 = \frac{x_3}{L} \quad (u'_1,u'_3) = (u_1,u_3)\frac{1}{L} \quad (u^{e\prime}_1, u^{e\prime}_3) = (u^e_1,u^e_3)\frac{1}{L} \quad \phi'_2 = \phi_2,\\ &\phi^{*\prime} = \phi^*, \quad t'_{ij} = \frac{1}{\nu T_0}t_{ij} \quad m'_{ij} = \frac{1}{L\nu T_0}m_{ij},\\ &\lambda^{*\prime}_i = \frac{1}{L\nu T_0}\lambda_i \quad q'_{ij} = \frac{1}{Lc_1\nu T_0}q_{ij}, \quad t^{e\prime}_{ij} = \frac{1}{\nu T_0}t^e_{ij}\\ &t' = \frac{c_1}{L}t, \quad T' = \frac{T}{T_0}, \quad w'_i = Lw_i, \quad L = \left(\frac{b}{\rho c^* T_0}\right)^{\frac{1}{2}}, \quad c_1^2 = \frac{\lambda+2\mu+K}{\rho}\end{aligned} \tag{13}$$

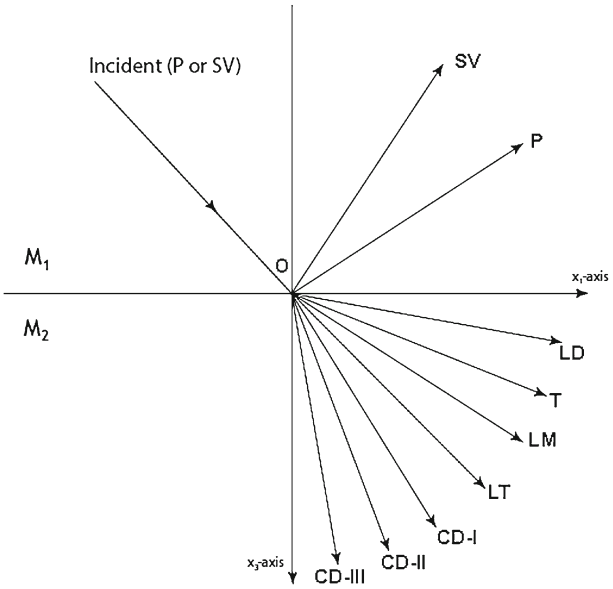

Fig. 1 Geometry of the problem

The relations connecting displacement components and microtemperature components to the potential functions in dimensionless form are

$$u_1 = \frac{\partial \phi}{\partial x_1} - \frac{\partial \psi}{\partial x_3}, \qquad u_3 = \frac{\partial \phi}{\partial x_3} + \frac{\partial \psi}{\partial x_1}, \quad w_1 = \frac{\partial \phi_1}{\partial x_1} - \frac{\partial \psi_1}{\partial x_3}, \qquad w_3 = \frac{\partial \phi_1}{\partial x_3} + \frac{\partial \psi_1}{\partial x_1} \tag{14}$$

where the primes have been suppressed.

Using the dimensionless quantities given by Eq. (13) in Eqs. (1)–(5) and with the aid of Eqs. (12) and (14), we obtain

$$\left[(a_1+1)\nabla^2 - a_5\frac{\partial^2}{\partial t^2}\right]\phi + a_3\phi^* - a_4 T = 0, \tag{15}$$

$$\left(\nabla^2 - a_5\frac{\partial^2}{\partial t^2}\right)\psi + a_2\phi_2 = 0, \tag{16}$$

$$\left(\nabla^2 - 2a_6 - a_8\frac{\partial^2}{\partial t^2}\right)\phi_2 - a_6\nabla^2\psi + a_7\nabla^2\psi_1 = 0, \tag{17}$$

$$\left(\nabla^2 - a_{10} - a_{13}\frac{\partial^2}{\partial t^2}\right)\phi^* - a_{11}\nabla^2\phi - a_{12}\nabla^2\phi_1 + a_9 T = 0, \tag{18}$$

$$\left(\nabla^2 - a_{14}\frac{\partial}{\partial t}\right)T - a_{15}\frac{\partial \phi^*}{\partial t} - a_{16}\nabla^2\phi + a_{17}\nabla^2\phi_1 = 0, \tag{19}$$

$$\left[\nabla^2(1+a_{18}) - a_{21} - a_{23}\frac{\partial}{\partial t}\right]\phi_1 - a_{20}\frac{\partial \phi^*}{\partial t} - a_{22}T = 0, \tag{20}$$

$$\left(\nabla^2 - a_{21} - a_{23}\frac{\partial}{\partial t}\right)\psi_1 + a_{19}\frac{\partial \phi_2}{\partial t} = 0, \tag{21}$$

where the values of a_i are given in Appendix 9.

Assuming the motion to be simple harmonic, we can write:

$$\{\phi, T, \phi^*, \phi_1, \psi, \phi_2, \psi_1\} = \{\overline{\phi}, , \overline{T}, \overline{\phi^*}, \overline{\phi_1}, \overline{\psi}, \overline{\phi_2}, \overline{\psi_1}\}\, e^{-\iota\omega t}, \tag{22}$$

where ω is the angular frequency, $\overline{\phi}$, $\overline{T}$, $\overline{\phi^*}$, $\overline{\phi_1}$, $\overline{\psi}$, $\overline{\phi_2}$, $\overline{\psi_1}$ are independent of time and are functions of coordinates x_1 and x_3. Using Eq. (22) into Eqs. (15)–(21), we obtain:

$$(a_1^*\nabla^2 + a_5\omega^2)\overline{\phi} + a_3\overline{\phi^*} - a_4\overline{T} = 0, \tag{23}$$

$$(\nabla^2 + a_5\omega^2)\overline{\psi} + a_2\overline{\phi_2} = 0, \tag{24}$$

$$(\nabla^2 - 2a_6 + a_8\omega^2)\overline{\phi_2} - a_6\nabla^2\overline{\psi} + a_7\nabla^2\overline{\psi_1} = 0, \tag{25}$$

$$(\nabla^2 - a_{10} + a_{13}\omega^2)\overline{\phi^*} - a_{11}\nabla^2\overline{\phi} - a_{12}\nabla^2\overline{\phi_1} + a_9\overline{T} = 0, \tag{26}$$

$$(\nabla^2 + a_{14}\iota\omega)\overline{T} + a_{15}\iota\omega\overline{\phi^*} - a_{16}\nabla^2\overline{\phi} + a_{17}\nabla^2\overline{\phi_1} = 0, \tag{27}$$

$$(\nabla^2 a_{18}^* - a_{21} + a_{23}\iota\omega)\overline{\phi_1} + a_{20}\iota\omega\overline{\phi^*} - a_{22}\overline{T} = 0, \tag{28}$$

$$(\nabla^2 - a_{21} + a_{23}\iota\omega)\psi_1 - a_{19}\iota\omega\overline{\phi_2} = 0, \tag{29}$$

Solving Eqs. (23), (26), (27) and (28), we obtain

$$[F_1(\nabla^2)^4 + F_2(\nabla^2)^3 + F_3(\nabla^2)^2 + F_4\nabla^2 + F_5]\overline{\phi} = 0, \tag{30}$$

where the values of F_i's are defined in Appendix 10.

The general solution of Eq. (30) can be written as

$$\overline{\phi} = \overline{\phi_1} + \overline{\phi_2} + \overline{\phi_3} + \overline{\phi_4}, \tag{31}$$

where the potentials $\overline{\phi_i}$; $i = 1, 2, 3, 4$ are solutions of wave equations, given by

$$\left[\nabla^2 + \frac{\omega^2}{V_i^2}\right]\overline{\phi_i} = 0, \qquad i = 1, 2, 3, 4. \tag{32}$$

Here, V_1, V_2, V_3, and V_4 are the velocities of four longitudinal waves, that is LD, T, LM, and LT waves, and are derived from the roots of biquadratic equations in V^2, given by

$$F_5V^8 - F_4\omega^2V^6 + F_3\omega^4V^4 - F_2\omega^6V^2 + F_1\omega^8 = 0, \tag{33}$$

Solving Eqs. (24), (25), and (29), we obtain

$$[(\nabla^2)^3 + F_6(\nabla^2)^2 + F_7\nabla^2 + F_8]\overline{\psi} = 0, \tag{34}$$

where $F_6 = (a_5 + a_8)\omega^2 + (-a_{23} + a_7a_{19})\iota\omega + a_{21} - a_6(2 - a_2)$, $F_7 = -a_5\omega^2(-a_{21} + a_{23}\iota\omega - a_8\omega^2 + 2a_6 - a_7a_{19}\iota\omega) + (-2a_6 + a_8\omega^2 + a_2a_6)(a_{21} - a_{23}\iota\omega)$, $F_7 = -a_5\omega^2(2a_6 - a_8\omega^2)(a_{21} - a_{23}\iota\omega)$,

The general solution of Eq. (34) can be written as

$$\overline{\psi} = \overline{\psi_5} + \overline{\psi_6} + \overline{\psi_7}, \tag{35}$$

where the potentials $\overline{\psi_i}$; $i = 5, 6, 7$ are solutions of wave equations, given by

$$\left[\nabla^2 + \frac{\omega^2}{V_i^2}\right]\overline{\psi_i} = 0, \qquad i = 5, 6, 7. \tag{36}$$

Here V_5, V_6, and V_7 are the velocities of three transverse waves, that is CD-I, CD-II, and CD-III waves, and are derived from the roots of cubic equations in V^2, given by

$$F_8V^6 - F_7\omega^2V^4 + F_6\omega^4V^2 - \omega^6 = 0, \tag{37}$$

Making use of Eq. (31) in Eqs. (23), (26), (27), and (28) and with the aid of Eqs. (22) and (32), the general solutions for ϕ, T, ϕ^*, ϕ_1 are obtained as

$$\{\phi, T, \phi^*, \phi_1\} = \sum_{i=1}^{4}\{1, n_i, m_i, k_i\}\phi_i, \tag{38}$$

Making use of Eq. (35) in Eqs. (24), (25), and (29) and with the aid of Eqs. (22) and (36), the general solutions for ψ, ϕ_2, ψ_1 are obtained as

$$\{\psi, \phi_2, \psi_1\} = \sum_{i=1}^{4} \{1, g_i, f_i\}\phi_i$$

where the values of n_i, m_i, k_i, g_i, f_i are given in Appendix 11.

Using the dimensionless quantities (13) in Eq. (10) with the aid of (12) and after suppressing the primes, we obtain

$$\frac{\left(\alpha^{e^2} - \beta^{e^2}\right)}{c_1^2}\frac{\partial}{\partial x_1}\left(\frac{\partial u_1^e}{\partial x_1} + \frac{\partial u_3^e}{\partial x_3}\right) + \frac{\beta^{e^2}}{c_1^2}\nabla^2 u_1 = \frac{\partial^2 u_1^e}{\partial t^2}, \tag{40}$$

$$\frac{(\alpha^{e^2} - \beta^{e^2})}{c_1^2}\frac{\partial}{\partial x_3}\left(\frac{\partial u_1^e}{\partial x_1} + \frac{\partial u_3^e}{\partial x_3}\right) + \frac{\beta^{e^2}}{c_1^2}\nabla^2 u_3 = \frac{\partial^2 u_3^e}{\partial t^2}, \tag{41}$$

where $\alpha^e = \sqrt{(\lambda^e + 2\mu^e)/\rho^e}$, $\beta^e = \sqrt{\mu^e/\rho^e}$ are velocities of longitudinal and transverse waves corresponding to medium M_1, respectively.

The components u_1^e and u_3^e are related by the potential functions as

$$u_1^e = \frac{\partial \phi^e}{\partial x_1} - \frac{\partial \psi^e}{\partial x_3}, \qquad u_3^e = \frac{\partial \phi^e}{\partial x_3} + \frac{\partial \psi^e}{\partial x_1}, \tag{42}$$

where ϕ^e and ψ^e satisfy the wave equations as

$$\nabla^2 \phi^e = \frac{1}{\alpha'^2}\frac{\partial^2 \phi^e}{\partial t^2}, \qquad \nabla^2 \psi^e = \frac{1}{\beta'^2}\frac{\partial^2 \psi^e}{\partial t^2}, \tag{43}$$

where $\alpha' = \frac{\alpha^e}{c_1}$, $\beta' = \frac{\beta^e}{c_1}$.

4 Reflection and refraction

We consider a harmonic (P-wave or SV-wave) propagating through an isotropic elastic solid half-space and is incident at the interface $x_3 = 0$ with its direction of propagation with angle θ_0 normal to the surface as shown in Fig. 1. Corresponding to each incident wave, we get reflected longitudinal wave (P-wave), transverse wave (SV-wave) in an isotropic elastic solid half-space (medium M_1), and refracted longitudinal displacement wave (LD-wave), thermal wave (T-wave), microstretch wave (LM-wave), microtemperature wave (LT-wave), transverse displacement wave coupled with microrotational wave, and microtemperature wave namely (CD-I wave, CD-II wave and CD-III wave) in medium M_2.

In an elastic solid half-space, the potential functions satisfying Eq. (43) are

$$\phi^e = A_0^e e^{[\iota\omega\{(x_1 \sin\theta_0 + x_3 \cos\theta_0)/\alpha' - t\}]} + A_1^e e^{[\iota\omega\{(x_1 \sin\theta_1 - x_3 \cos\theta_1)/\alpha' - t\}]}, \tag{44}$$

$$\psi^e = B_0^e e^{[\iota\omega\{(x_1 \sin\theta_0 + x_3 \cos\theta_0)/\beta' - t\}]} + B_1^e e^{[\iota\omega\{(x_1 \sin\theta_2 - x_3 \cos\theta_2)/\beta' - t\}]}, \tag{45}$$

The coefficients A_0^e, B_0^e, A_1^e, and B_1^e represent the amplitudes of the incident P (or SV), reflected P, and reflected SV-waves, respectively.

Following Borcherdt [45], in an isotropic microstretch thermoelastic solid half-space with microtemperatures, the potential functions satisfying Eqs. (32) and (36) are

$$\{\phi, T, \phi^*, \phi_1\} = \sum_{i=1}^{4} \{1, n_i, m_i, k_i\} B_i e^{(\mathbf{A}_i \cdot \mathbf{r})} e^{\{\iota(\mathbf{P}_i \cdot \mathbf{r} - \omega t)\}}, \tag{46}$$

$$\{\psi, \phi_2, \psi_1\} = \sum_{j=5}^{7} \{1, g_j, l_j\} B_j e^{(\mathbf{A}_j \cdot \mathbf{r})} e^{\{\iota(\mathbf{P}_j \cdot \mathbf{r} - \omega t)\}}, \tag{47}$$

The coefficients $B_i, i = 1, 2, 3, 4, 5, 6, 7$ represent the amplitudes of transmitted LD, T, LM, LT, CD-I, CD-II, and CD-III waves, respectively. The propagation vector $P_i, i = 1, 2, 3, 4, 5, 6, 7$ and the attenuation vector $A_i, i = 1, 2, 3, 4, 5, 6, 7$

$$\mathbf{P}_i = \xi_R \hat{x_1} + dV_{iR} \hat{x_3}, \qquad \mathbf{A}_i = -\xi_I \hat{x_1} - dV_{iI} \hat{x_3}, \quad i = 1, 2, 3, 4, 5, 6, 7 \tag{48}$$

where

$$dV_i = dV_{iR} + dV_{iI} = p.v.\left(\frac{\omega^2}{V_i^2} - \xi^2\right)^{1/2}; \quad i = 1, 2, 3, 4, 5, 6, 7 \tag{49}$$

and $\xi = \xi_R + \iota\xi_I$ is a complex wave number. The subscripts R and I denote the real and imaginary parts of the corresponding complex quantity, and $p.v.$ stands for the principal value of the complex quantity obtained after square root. The inequality $\xi_R \geq 0$ ensures propagation in the positive x_1- direction. The complex wave number ξ in microstretch thermoelastic solid half-space with microtemperatures is

$$\xi = |\mathbf{P}_i| \sin\theta_i' - \iota\,|\mathbf{A}_i| \sin(\theta_i' - \gamma_i), \quad i = 1, 2, 3, 4, 5, 6, 7 \tag{50}$$

where $\gamma_i, i = 1, 2, 3, 4, 5, 6, 7$ is the angle between the propagation and the attenuation vectors and $\theta_i', i = 1, 2, 3, 4, 5, 6, 7$ is the angle of refraction in medium M_2.

5 Boundary conditions

The boundary conditions at the interface $x_3 = 0$ are $t_{33} = t_{33}^e,\ t_{31} = t_{31}^e,\ m_{32} = 0,\ \lambda_3^* = 0, q_{33} = 0, q_{31} = 0, u_3 = u_3^e,\ u_1 = u_1^e,$

$$\frac{\partial T}{\partial x_3} = 0 \tag{51}$$

Making the use of potentials given by Eqs. (46), (47), we find that the boundary conditions are satisfied if and only if:

$$\xi_R = \frac{\omega \sin\theta_0}{V_0} = \frac{\omega \sin\theta_1}{\alpha'} = \frac{\omega \sin\theta_2}{\beta'}, \tag{52}$$

and

$$\xi_I = 0, \tag{53}$$

where $V_0 = \alpha'$, for incident P-wave and $V_0 = \beta'$, for incident SV-wave

Making use of Eqs. (44)–(47) in boundary conditions (51) and with the help of Eqs. (52) and (53), we obtain a system of nine non-homogeneous equations

$$\sum_{j=1}^{9} a_{ij} Z_j = Y_i; \quad (i = 1, 2, 3, 4, 5, 6, 7, 8, 9) \tag{54}$$

where the values of a_{ij} are given in Appendix 12.

(1) For incident P-wave:

$$A^* = A_0^e, \quad B_0^e = 0, \quad Y_1 = -a_{11} \quad Y_2 = a_{21}\,, \quad Y_3 = 0, \quad Y_4 = 0,$$
$$Y_5 = 0, \quad Y_6 = a_{61}, \quad Y_7 = a_{71}, \quad Y_8 = -a_{81}, \quad Y_9 = 0$$

(2) For incident SV-wave:

$$A^* = B_0^e, \quad A_0^e = 0, \quad Y_1 = -a_{12} \quad Y_2 = a_{22}, \quad Y_3 = 0, \quad Y_4 = 0,$$
$$Y_5 = 0, \quad Y_6 = a_{62}, \quad Y_7 = a_{72}, \quad Y_8 = -a_{82}, \quad Y_9 = 0$$

and

$$Z_1 = \frac{A_1^e}{A^*}, \quad Z_2 = \frac{B_1^e}{A^*}, \quad Z_3 = \frac{B_1}{A^*}, \quad Z_4 = \frac{B_2}{A^*}, \quad Z_5 = \frac{B_3}{A^*}, \quad Z_6 = \frac{B_4}{A^*}, \quad Z_7 = \frac{B_5}{A^*},$$
$$Z_8 = \frac{B_6}{A^*}, Z_9 = \frac{B_7}{A^*}$$

where $Z_1,\ Z_2$ are the amplitude ratios of reflected P-wave, SV-wave medium M_1 and $Z_3,\ Z_4,\ Z_5,\ Z_6,\ Z_7,$ Z_8, Z_9 are the amplitude ratios of refracted LD-wave, T-wave, LM-wave, LT-wave, and coupled CD-I, CD-II, and CD-III waves in medium M_2.

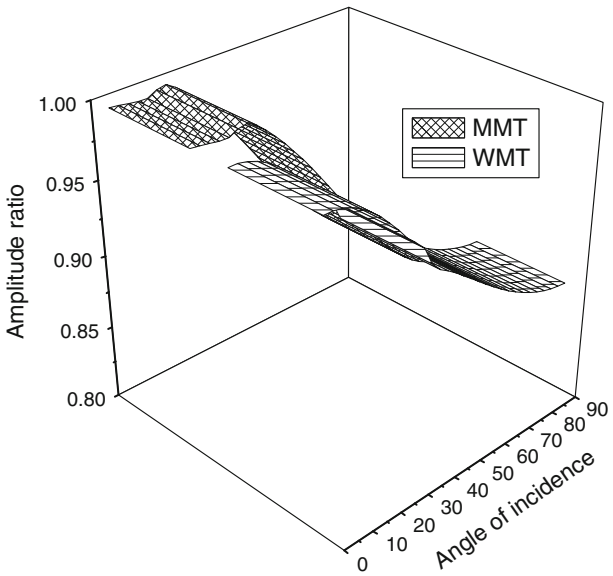

Fig. 2 Variation of $|Z_1|$ with the angle of incidence (P-wave)

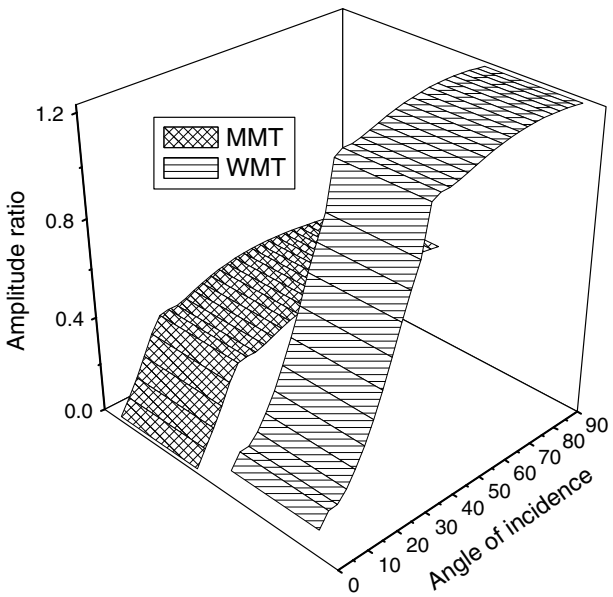

Fig. 3 Variation of $|Z_2|$ with the angle of incidence (P-Wave)

6 Particular cases

(a) If we neglect micropolarity effect in medium M_2, i.e., $K = 0$, then we obtain amplitude ratios at an interface of an elastic solid half-space and microstretch thermoelastic solid half-space with microtemperatures without microrotational effect as

$$\sum_{j=1}^{8} a_{ij} Z_j = Y_i; \quad (i = 1, 2, 3, 4, 5, 6, 7, 8) \tag{55}$$

where the values of a_{ij} are given in Appendix 13.

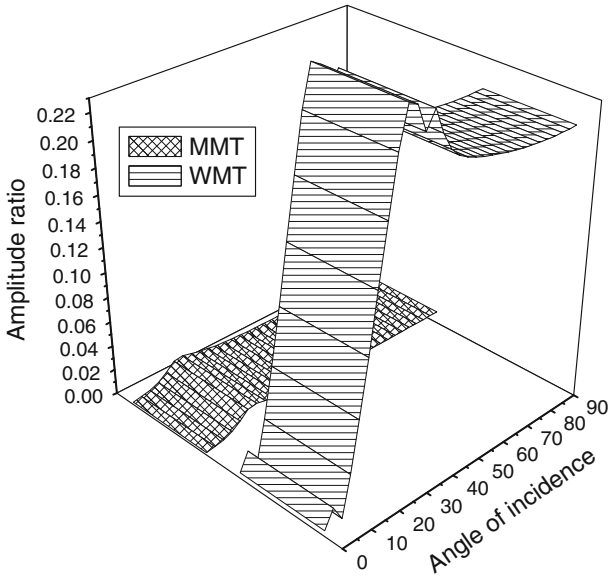

Fig. 4 Variation of $|Z_3|$ with the angle of incidence (P-wave)

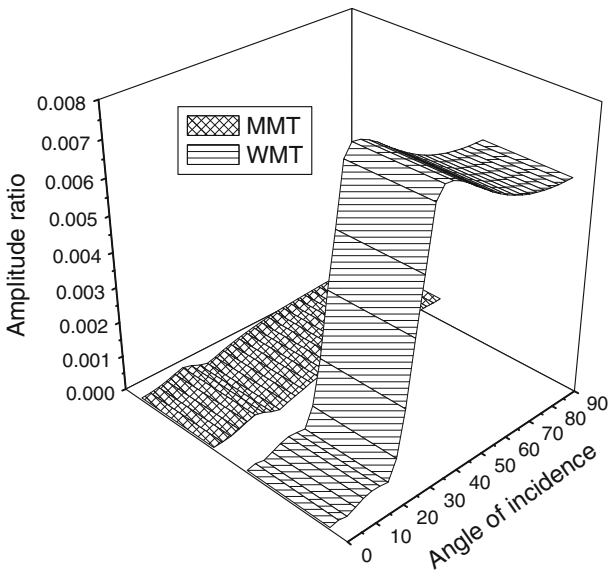

Fig. 5 Variation of $|Z_4|$ with the angle of incidence (P-Wave)

7 Numerical results and discussion

The following values of relevant parameters are taken for numerical computations.

Following Eringen [46], the values of micropolar constants are

$$\lambda = 9.4 \times 10^{10}\,\mathrm{Nm}^{-2}, \quad \mu = 4.0 \times 10^{10}\,\mathrm{Nm}^{-2},$$
$$K = 1.0 \times 10^{10}\,\mathrm{Nm}^{-2}, \quad \gamma = 7.79 \times 10^{-10}\,\mathrm{N},$$
$$j = 0.0000002 \times 10^{-14}\,\mathrm{m}^2, \quad \rho = 1.74 \times 10^{3}\,\mathrm{Kgm}^{-3}.$$

and thermal parameters are [47]:

$$c^* = 0.104 \times 10^{4}\,\mathrm{NmKg}^{-1}\,\mathrm{K}^{-1},$$
$$T_0 = 298\,\mathrm{K}, \qquad K^* = 1.7 \times 10^{2}\,\mathrm{Nsec}^{-1}\,\mathrm{K}^{-1}, \qquad \tau_1 = 0.613 \times 10^{3}\,\mathrm{s}.$$

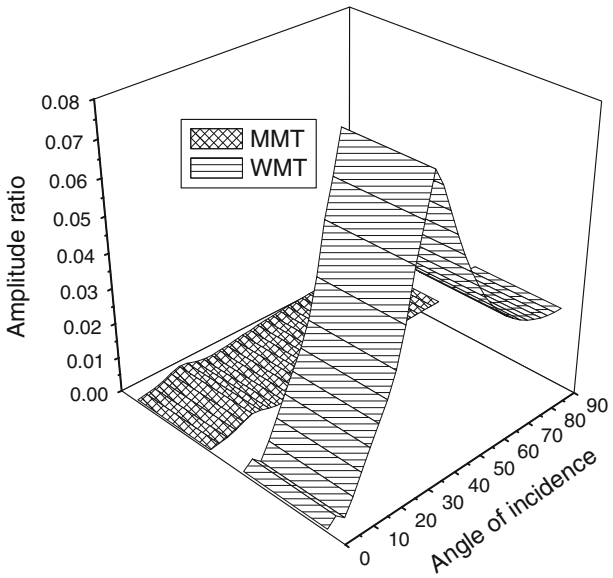

Fig. 6 Variation of $|Z_5|$ with the angle of incidence (P-wave)

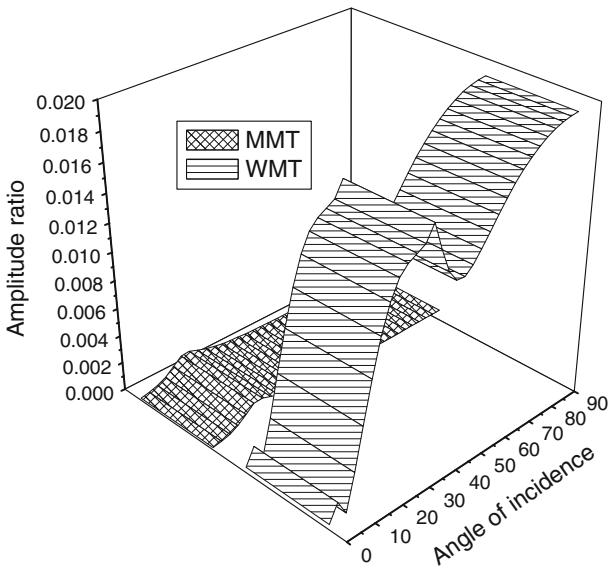

Fig. 7 Variation of $|Z_6|$ with the angle of incidence (P-Wave)

Microstretch parameters are

$j_0 = 0.000019 \times 10^{-13}\,\mathrm{m}^2$, $b = 0.15 \times 10^{-10}\,\mathrm{N}$, $\lambda_0 = 0.21 \times 10^{11}\,\mathrm{Nm}^{-2}$, $\lambda_1 = 0.007 \times 10^{12}\,\mathrm{Nm}^{-2}$, $\alpha_0 = 0.008 \times 10^{-7}\,\mathrm{N}$.

and microtemperatures parameters are

$k_1 = 0.0035\,\mathrm{Ns}^{-1}$, $k_2 = 0.045\,\mathrm{Ns}^{-1}$, $k_3 = 0.055\,\mathrm{NK}^{-1}\mathrm{s}^{-1}$, $k_4 = 0.065\,\mathrm{Ns}^{-1}\mathrm{m}^2$, $k_5 = 0.076\,\mathrm{Ns}^{-1}\mathrm{m}^2$, $k_6 = 0.096\,\mathrm{Ns}^{-1}\mathrm{m}^2$, $\mu_1 = 0.0085\,\mathrm{N}$, $\mu_2 = 0.0095\,\mathrm{N}$.

Following Bullen [44], the numerical data of granite in elastic medium are

$$\rho^e = 2.65 \times 10^3\,\mathrm{Kgm}^{-3}, \quad \alpha^e = 5.27 \times 10^3\,\mathrm{ms}^{-1}, \quad \beta^e = 3.17 \times 10^3\,\mathrm{ms}^{-1}.$$

The values of amplitude ratios for incidence of P-wave and SV-wave have been computed at different angles of incidence. In Figs. 2, 3, 4, 5, 6, 7, 8, 9, 10, 11, 12, 13, 14, 15, 16, 17, 18, and 19, MMT corresponds to

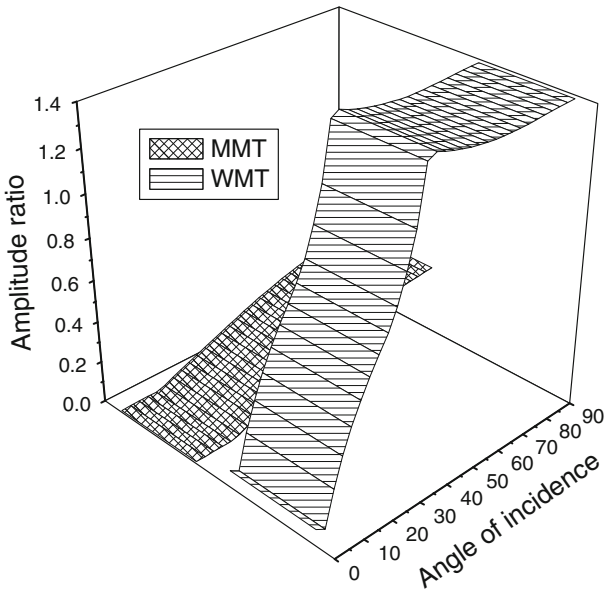

Fig. 8 Variation of $|Z_7|$ with the angle of incidence (P-wave)

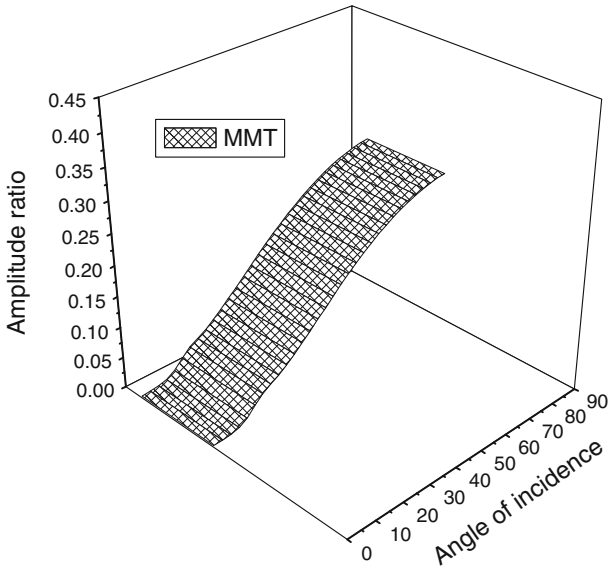

Fig. 9 Variation of $|Z_8|$ with the angle of incidence (P-Wave)

microstretch thermoelastic solid with microtemperatures and WMT corresponds to microstretch thermoelastic solid with microtemperatures without microrotational effect.

7.1 Incident P-Wave

Variations of amplitude ratios $|Z_i|$; $1 \leq i \leq 9$ with the angle of incidence θ_0, for incident P-wave are shown in Figs. 2, 3, 4, 5, 6, 7, 8, 9, and 10.

It is clear from Fig. 2 that the values of amplitude ratio $|Z_1|$ for MMT increase in the range $0^\circ < \theta_0 < 20^\circ$ and then decrease in the further range, while the values for WMT decrease monotonically with increase in θ_0. It is noticed that the values for MMT are greater than the values for WMT in the whole range, except the initial range $0^\circ < \theta_0 < 8^\circ$ which shows that the effect of micropolarity increases the magnitude of amplitude ratio with increase in θ_0.

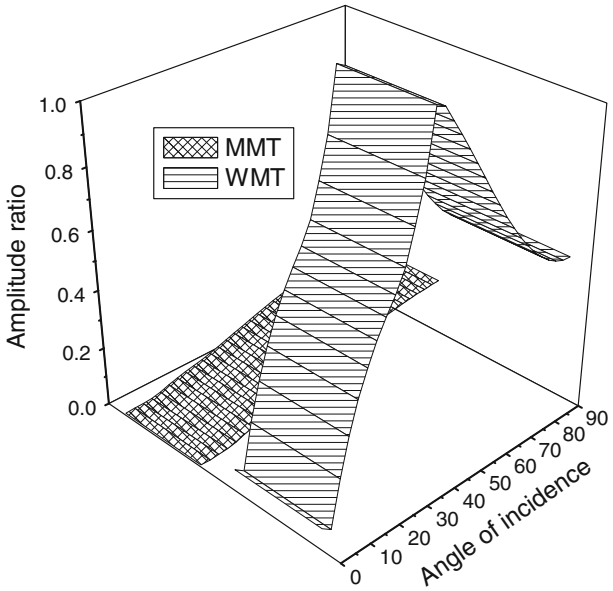

Fig. 10 Variation of $|Z_9|$ with the angle of incidence (P-wave)

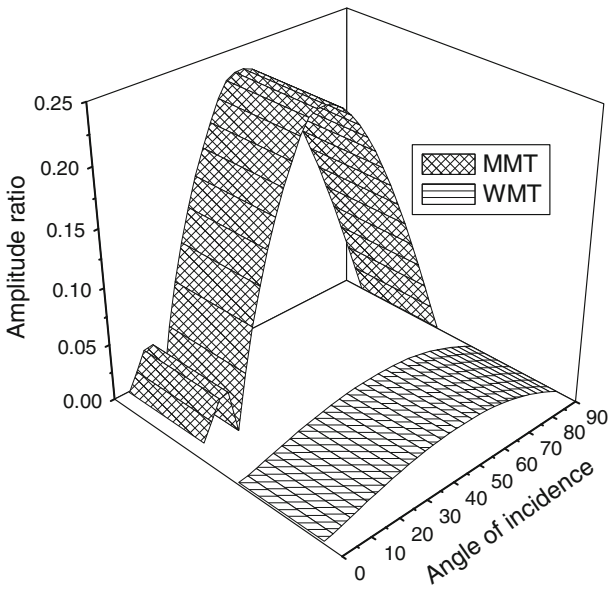

Fig. 11 Variation of $|Z_1|$ with the angle of incidence (SV-Wave)

It is evident from Fig. 3 that the values of amplitude ratio $|Z_2|$ for MMT increase in range $0° < \theta_0 < 55°$ and the values of amplitude ratio decrease with further increase in θ_0. The values for WMT start with minimum value at the normal incidence and then increase with angle of incidence upto $\theta_0 < 78°$, and in the further range, the magnitude of amplitude ratio decrease. The values for WMT in comparison with MMT are greater in the whole range, except the initial range, where the behavior is reversed.

Figure 4 shows that the values of amplitude ratio $|Z_3|$ for MMT increase in the intervals $8° < \theta_0 < 20°$, $68° < \theta_0 < 90°$ and decrease in the interval $20° < \theta_0 < 68°$. The values for WMT oscillate in the whole range and attain maximum value in the range $8° < \theta_0 < 20°$.

Figure 5 indicates that the values of amplitude ratio $|Z_4|$ in the absence of micropolarity effect are greater than the values in the presence of micropolarity effect. The amplitude ratio in the absence of micropolarity effect attains maximum value in the range $37° < \theta_0 < 41°$. It is clear from Fig. 6 that the behavior of oscillation of $|Z_5|$ is similar to $|Z_4|$ with difference in their magnitude values.

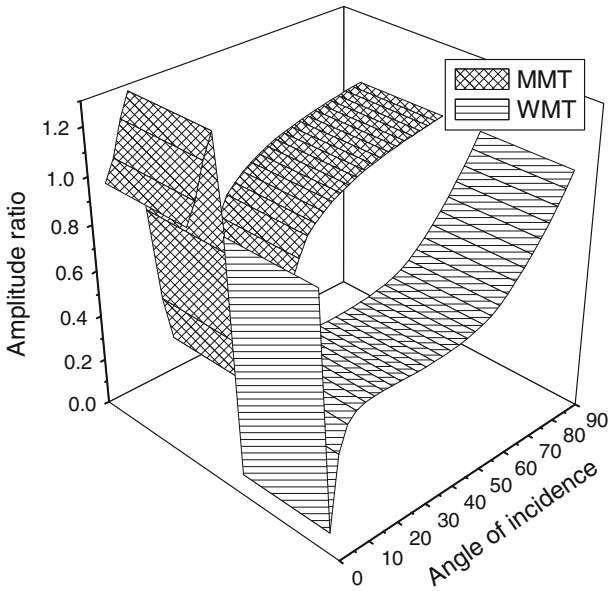

Fig. 12 Variation of $|Z_2|$ with the angle of incidence (SV-Wave)

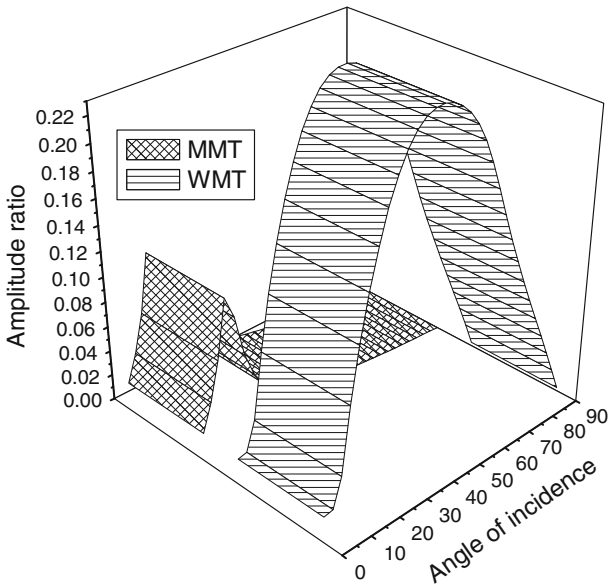

Fig. 13 Variation of $|Z_3|$ with the angle of incidence (SV-wave)

Figure 7 shows that the values of $|Z_6|$ for MMT increase in the range $0^\circ < \theta_0 < 20^\circ$ to attain maximum value, then decrease in the range $20^\circ < \theta_0 < 55^\circ$ and again increases in the further range. The values of amplitude ratio for WMT attain maximum value at the grazing incidence. In this case, the micropolarity effect decreases the magnitude of amplitude ratio.

It is noticed from Fig. 8 that the values of $|Z_7|$ for MMT start with minimum value at the grazing incidence and then increase to attain maximum value at the grazing incidence. It is seen that the values for WMT decrease in the initial range $0^\circ < \theta_0 < 5^\circ$ and then increase sharply upto $\theta_0 < 41^\circ$ and the values of amplitude ratio fluctuate in the further range. The values for WMT are greater than the values for MMT in the whole range that reveals the effect of micropolarity.

It is noticed from Fig. 9 that values of amplitude ratio $|Z_8|$ for WMT get increased from normal incidence to grazing incidence. Figure 10 depicts that the values of amplitude ratio $|Z_9|$ for WMT show fluctuating

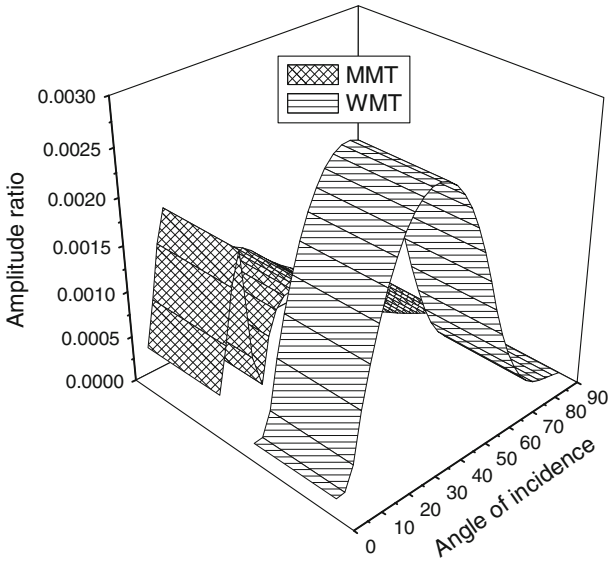

Fig. 14 Variation of $|Z_4|$ with the angle of incidence (SV-Wave)

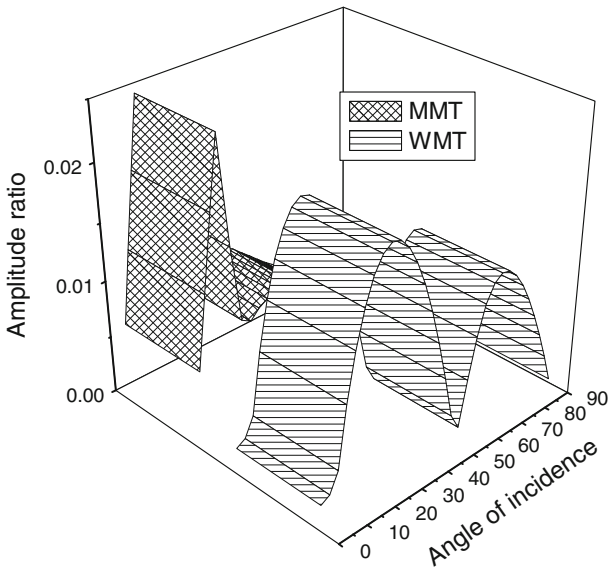

Fig. 15 Variation of $|Z_5|$ with the angle of incidence (SV-wave)

behavior in the whole range and attain maximum value in the range $34° < \theta_0 < 37°$. On the other hand, the values for MMT increase rapidly from $\theta_0 = 0°$ from $\theta_0 = 90°$.

7.2 Incident SV-Wave

Variations of amplitude ratios $|Z_i|$; $1 \leq i \leq 9$ with the angle of incidence θ_0, for incident SV-wave are shown in Figs. 11, 12, 13, 14, 15, 16, 17, 18 and 19.

From Fig. 11, it is evident that the values of $|Z_1|$ for MMT increase slowly till $\theta_0 < 10°$, and afterward, it decreases very slowly upto $\theta_0 < 13°$. Beyond $\theta_0 \geq 13°$, the amplitude increases very smoothly till $\theta_0 < 46°$, and thereafter, it decreases frequently and attains minimum value at the grazing incidence. The amplitude ratio for WMT increase with angle of incidence till $\theta_0 < 52°$; then, it gradually decreases upto grazing incidence. Moreover, the values of amplitude ratio for MMT are greater than the values for WMT in the whole range.

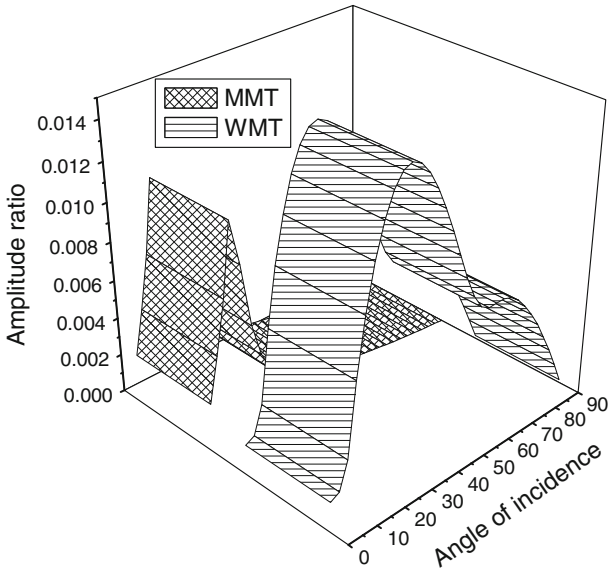

Fig. 16 Variation of $|Z_6|$ with the angle of incidence (SV-Wave)

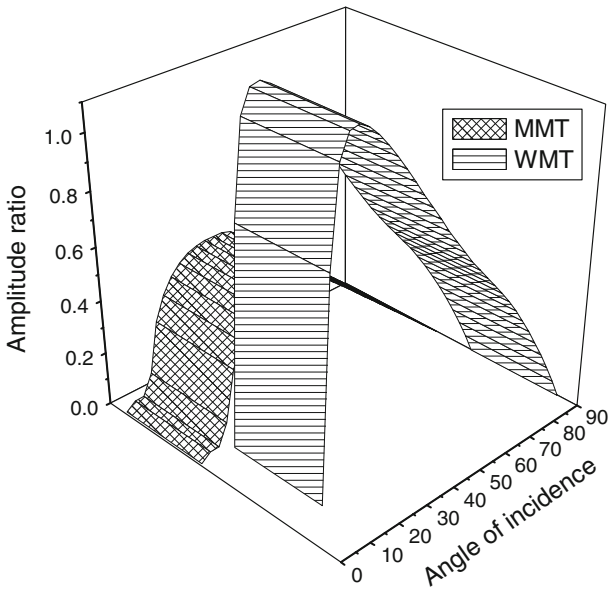

Fig. 17 Variation of $|Z_7|$ with the angle of incidence (SV-wave)

It is clear from Fig. 12 that the values of $|Z_2|$ for MMT increase slowly till $\theta_0 = 10°$, and afterward, its value decrease gradually in the range $10° < \theta_0 < 22°$. After $\theta_0 = 22°$, the values of $|Z_2|$ increase. On the other hand, the values for WMT decrease gradually in the range $0° < \theta_0 < 5°$ and then increase till grazing incidence.

Figure 13 indicates that the values of amplitude ratio $|Z_3|$ for MMT firstly show oscillating behavior in range $0° < \theta_0 < 28°$ and then decrease continuously in the further range. It is seen that the values of amplitude ratio for WMT increase in the range $0° < \theta_0 < 37°$ and then decrease with further increase in angle of incidence. In this case, the micropolarity effect increases the magnitude of amplitude ratio near the normal and grazing incidence.

It is noticed from Fig. 14 that values of $|Z_4|$ for MMT increase in the range $0° < \theta_0 < 50°$ and then decrease in the further range. It is evident that the values for WMT decrease sharply in the whole range and are greater in comparison with the values for MMT in the range $0° < \theta_0 < 37°$ and behavior is opposite in the remaining range.

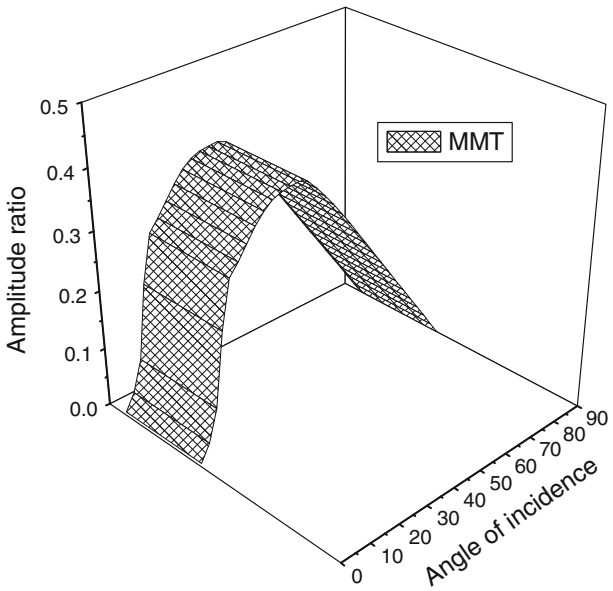

Fig. 18 Variation of $|Z_8|$ with the angle of incidence (SV-Wave)

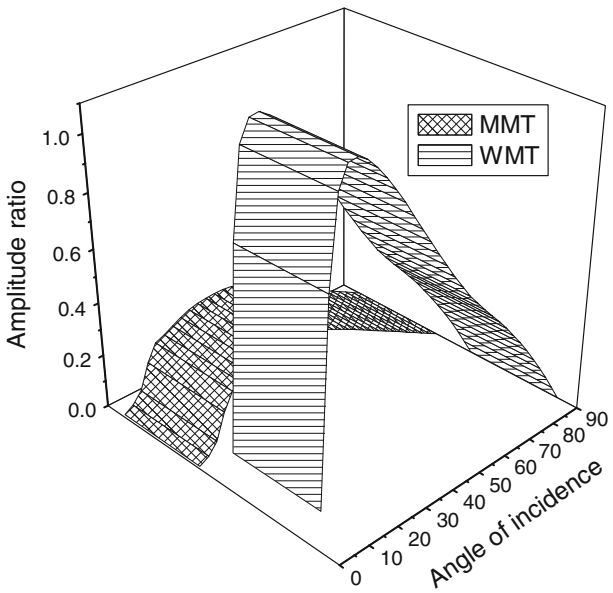

Fig. 19 Variation of $|Z_9|$ with the angle of incidence (SV-wave)

Figure 15 depicts that the amplitude $|Z_5|$ begins with the value 0.00698 near the normal incidence, it increases till $\theta_0 = 10°$, and afterward, it decreases gradually upto $\theta_0 = 19°$. Beyond $\theta_0 = 19°$, the amplitude increases very smoothly till $\theta_0 = 31°$, and thereafter, it decreases frequently and attains the minimum value.

It is clear from Fig. 16 that the values of $|Z_6|$ for MMT increase slowly with increase in angle of incidence till $\theta_0 = 10°$; then, its value decreases till $\theta_0 = 90°$. The value of amplitude ratio $|Z_6|$ increases with increase in the angle of incidence till $\theta_0 = 28°$, and then, it gradually decreases to attain minimum value at grazing incidence.

Figure 17 shows that the values of $|Z_7|$ for MMT increase in the range $0° < \theta_0 < 34°$ and attain maximum value. Afterward, its value decreases to attain minimum value at the grazing incidence. Moreover, the values for WMT increase gradually with angle of incidence till $\theta_0 = 13°$, and thereafter, its value decreases sharply as θ_0 approaches to 90°. The micropolarity effect decreases the magnitude of amplitude ratio $|Z_7|$. Figure 18 indicates that the values of amplitude ratio $|Z_8|$ for WMT increase with increase in angle of incidence and attain their maximum values near $\theta_0 = 37°$. Thereafter, they decrease and attain minimum value at grazing incidence.

Figure 8 shows that initially, the values of amplitude ratio $|Z_9|$ for MMT increase with increase in angle of incidence till $\theta_0 = 40°$, and then, it gradually decreases till grazing incidence. The values of amplitude ratio for WMT increase gradually till $\theta_0 = 13°$ and then decreases to attain minimum value at the grazing incidence.

8 Conclusion

The reflection and refraction coefficients at the interface of an elastic solid half-space and microstretch thermoelastic solid half-space with microtemperatures have been discussed in the present article. The amplitude ratios of various reflected and refracted waves have been calculated numerically and their variations have been shown graphically with respect to angle of incidence. It is concluded that for incidence of SV-wave, the values for WMT (without microrotational effect) are smaller as compared to the values for MMT (with microrotational effect). The values of amplitude ratio of refracted LD, LT, CD-I, and CD-II waves in the absence of micropolarity effect are greater than the values in presence of micropolarity effect that reveals the effect of microrotation (when P-wave is incident). It is clearly depicted that when P-wave is incident, the values of amplitude ratios in the absence of microrotations effect are more oscillatory near the normal incidence and grazing incidence due to the complex structure. It is noticed that microrotational effect becomes more prominent with increase in angle of incidence. The above problem is of geophysical interest and finds applications in the problems related to seismology.

9 Appendix I

$$a_1 = \tfrac{\lambda+\mu}{\mu+K},\quad a_2 = \tfrac{K}{\mu+K},\quad a_3 = \tfrac{\lambda_0}{\mu+K},\quad a_4 = \tfrac{\nu T_0}{\mu+K},\quad a_5 = \tfrac{\rho c_1^2}{\mu+K},\quad a_6 = \tfrac{KL^2}{\gamma},$$
$$a_7 = \tfrac{\mu_1}{\gamma},\quad a_8 = \tfrac{\rho j c_1^2}{\gamma},\quad a_9 = \tfrac{\nu_1 T_0 L^2}{\alpha_0},\quad a_{10} = \tfrac{\lambda_1 L^2}{\alpha_0},\quad a_{11} = \tfrac{\lambda_0 L^2}{\alpha_0},\quad a_{12} = \tfrac{\mu_2}{\alpha_0},\quad a_{13} = \tfrac{\rho j_0 c_1^2}{2\alpha_0},$$
$$a_{14} = \tfrac{\rho c^* c_1 L}{K^*},\quad a_{15} = \tfrac{\nu_1 c_1 L}{K^*},\quad a_{16} = \tfrac{\nu c_1 L}{K^*},\quad a_{17} = \tfrac{k_1}{K^* T_0},\quad a_{18} = \tfrac{k_4+k_5}{k_6},\quad a_{19} = \tfrac{\mu_1 c_1 L}{k_6},$$
$$a_{20} = \tfrac{\mu_2 c_1 L}{k_6},\quad a_{21} = \tfrac{k_2 L^2}{k_6},\quad a_{22} = \tfrac{k_3 T_0 L^2}{k_6},\quad a_{23} = \tfrac{b c_1 L}{k_6}$$

10 Appendix II

$$F_1 = a_1^* a_{17} a_{18}^*,\quad F_2 = a_{18}^*(a_5\omega^2 a_{17} + a_1^*\delta_2 - a_3 a_{12} a_{16} + a_3\delta_1 - a_4 a_{16} a_{17}) + a_1^*(a_{17}\delta_6 - a_{12}\delta^*)$$
$$F_3 = a_5\omega^2\delta_7 - a_1^*\delta_5(a_{12} + \delta_3) + a_3\delta_8 - a_{18}^*\delta_3\delta_9 + a_4 a_{17}\delta_4 - \delta_3 a_1^*\delta^*,$$
$$F_4 = a_{14}^* a_{21}^*\delta_{10} + \delta_4\delta_{11} + \delta_5\delta_{12} - a_5\omega^2\delta_3\delta^*,\ F_3 = a_5\omega^2\delta_2 a_{21}^* a_{14}^*,$$
$$a_1^* = a_1 + 1,\quad a_{13}^* = a_{13}\omega^2 - a_{10},\quad a_{14}^* = a_{14}\iota\omega, a_{15}^* = a_{15}\iota\omega,\quad a_{18}^* = a_{18} + 1, a_{20}^* = a_{20}\iota\omega,$$
$$a_{21}^* = a_{23}\iota\omega - a_{21},$$
$$\delta_1 = a_{22}a_{17} + a_{21}^* + a_{18}^*(a_{14}^* + a_{13}^*), \delta_2 = a_{12}a_{22}a_{15}^* + a_{20}^* + a_9(a_{17}a_{20}^* - a_{15}^* a_{18}^*) + a_{21}^* a_{14}^*,$$
$$\delta_3 = [a_{22}a_{17} + a_{21}^* + a_{14}^*(a_{18}^* - a_{21}^*)]a_{13}^* + a_9 a_{15}^* a_{21}^* - a_{20}^* a_{14}^*,$$
$$\delta_4 = [a_{22}a_{17} + a_{21}^* + a_{14}^* a_{18}^*]a_{11} - a_9 a_{18}^* a_{16} + a_{12}a_{16}a_{22},$$
$$\delta_5 = [a_9 a_{16} - a_{14}^* a_{11}]a_{21}^*, \delta_6 = a_{21}^* a_{15}^* a_{11} + a_{17}a_{20}^* - a_{16}a_{13}^* a_{21}^*,$$
$$\delta_7 = [\delta_2 a_{18}^* - \delta^* a_{12}]a_{17}\delta_6, \delta_8 = a_{12}\delta_4 + \delta_1\delta_6,$$
$$\delta_9 = a_3 a_{16} - a_4 a_{16}\delta_2 a_{18}^* - \delta_1 a_4\delta^*,$$
$$\delta_{10} = a_1^*\delta_2 + a_3\delta_1, \delta_{11} = -a_3\delta_3 + a_4\delta_2, \delta_{12} = a_4\delta_1 - a_5\omega^2 a_{12} - a_5\omega^2\delta_3,$$

11 Appendix III

$$m_i = \frac{-\delta_1\frac{\omega^2}{V_i^2}\left[\left(a_{21}^* - a_{18}^*\frac{\omega^2}{V_i^2}\right)\left(-\frac{\omega^2}{V_i^2} + a_{14}^*\right) - a_{22}a_{17}a_{21}^*\right] + a_{16}\frac{\omega^2}{V_i^2}\left(a_{21}^* - a_{18}^*\frac{\omega^2}{V_i^2}\right)\left(\delta_3 - a_{12}a_{18}^*\frac{\omega^2}{V_i^2}\right)}{\left(\delta_2 - a_{17}\frac{\omega^2}{V_i^2}\right)\left[\left(a_{21}^* - a_{18}^*\frac{\omega^2}{V_i^2}\right)\left(-\frac{\omega^2}{V_i^2} + a_{14}^*\right) + a_{22}a_{17}\frac{\omega^2}{V_i^2}\right] + \left(\delta^*\frac{\omega^2}{V_i^2} - \delta_5\right)\left(\delta_3 - a_{12}\frac{\omega^2}{V_i^2}\right)},$$

$$k_i = \frac{\frac{\omega^2}{V_i^2}\left[a_{16}a_9 - a_{11}\left(-\frac{\omega^2}{V_i^2} + a_{14}^*\right)\right](a_3a_{22} - a_4a_{20}^*) + \left(a_5\omega^2 - a_1^*\frac{\omega^2}{V_i^2}\right)a_{22}\left[b_i\left(-\frac{\omega^2}{V_i^2} + a_{14}^*\right) - a_{15}^*a_9\right]}{a_4\left(-a_{18}^*\frac{\omega^2}{V_i^2} + a_{21}^*\right)\left[\left(-\frac{\omega^2}{V_i^2} + a_{14}^*\right)b_i - a_{15}^*a_9\right] + \frac{\omega^2}{V_i^2}(a_3a_{22} - a_4a_{20}^*)\left(\delta_3 - a_{12}\frac{\omega^2}{V_i^2}\right)},$$

$$b_i = \left(-\frac{\omega^2}{V_i^2} - a_{10} + a_{13}\omega^2\right),$$

$$n_i = \frac{\{-\delta_1\frac{\omega^2}{V_i^2}\left(\delta_5 - \delta^*\frac{\omega^2}{V_i^2}\right) + a_{16}\frac{\omega^2}{V_i^2}\left(a_{21}^* - a_{18}^*\frac{\omega^2}{V_i^2}\right)\left(\delta_2 - a_{17}\frac{\omega^2}{V_i^2}\right)\}}{\left(\delta_3 - a_{12}\frac{\omega^2}{V_i^2}\right)\left(\delta_5 - \delta^*\frac{\omega^2}{V_i^2}\right) - \left[-a_{22}a_{17}\frac{\omega^2}{V_i^2} + \left(a_{21}^* - a_{18}^*\frac{\omega^2}{V_i^2}\right)\left(a_{14}^* - \frac{\omega^2}{V_i^2}\right)\right]\left(\delta_2 - a_{17}\frac{\omega^2}{V_i^2}\right)},$$

$$l_j = \frac{-\iota a_{19}a_6\frac{\omega^3}{V_j}}{-a_7a_{19}\iota\frac{\omega^3}{V_j^2} + \left(-\frac{\omega^2}{V_j^2} + a_{21}^*\right)\left(-2a_6 - \frac{\omega^2}{V_j^2} + a_8\omega^2\right)},$$

$$g_j = \frac{\frac{\omega^2}{V_j^2}\left[\iota\omega a_7a_{19}\left(-\frac{\omega^2}{V_j^2} + a_5\omega^2\right) + a_2a_6\left(-\frac{\omega^2}{V_j^2} + a_{21}^*\right)\right]}{a_2\left(-2a_6 - \frac{\omega^2}{V_j^2} + a_8\omega^2\right)\left(-\frac{\omega^2}{V_j^2} + a_{21}^*\right)}$$

12 Appendix IV

$$a_{11} = \left[\overline{d_1}\frac{dV_{\alpha'}^2}{\omega^2} + \overline{d_2}\frac{\xi_R^2}{\omega^2}\right], \quad a_{12} = -\left(\overline{d_1} - \overline{d_2}\right)\frac{\xi_R}{\omega}\frac{dV_{\beta'}}{\omega},$$

$$a_{1l} = -d_1\frac{dV_{i'}^2}{\omega^2} - d_2\frac{\xi_R^2}{\omega^2} + d_3\frac{m_i}{\omega^2}, \quad a_{1k} = -(d_1 - d_2)\frac{\xi_R}{\omega}\frac{dV_j}{\omega},$$

$$a_{21} = 2\overline{d_3}\frac{\xi_R}{\omega}\frac{dV_{\alpha'}}{\omega}, \quad a_{22} = \overline{d_3}\left(\frac{dV_{\beta'}^2}{\omega^2} - \frac{\xi_R^2}{\omega^2}\right), \quad a_{2l} = (2d_4 + d_5)\frac{dV_i}{\omega}\frac{\xi_R}{\omega},$$

$$a_{2k} = -(d_4 + d_5)\frac{dV_{j'}^2}{\omega^2} + d_4\frac{\xi_R^2}{\omega^2} + d_5\frac{g_j}{\omega^2},$$

$$a_{31} = a_{32} = 0, \quad a_{3l} = \iota d_7m_i\frac{\xi_R}{\omega}, \quad a_{3k} = \iota d_6g_j\frac{d\mathrm{V}_j}{\omega},$$

$$a_{41} = a_{42} = 0, \quad a_{4l} = \iota d_8m_i\frac{d\mathrm{V}_i}{\omega}, \quad a_{4k} = -\iota d_9g_j\frac{\xi_R}{\omega},$$

$$a_{51} = a_{52} = 0, \quad a_{5l} = \left[-d_{10}\frac{\xi_R^2}{\omega^2} - (d_{10} + d_{11})\frac{dV_{i'}^2}{\omega^2}\right]k_i, \quad a_{5k} = -d_{11}l_j\frac{\xi_R}{\omega}\frac{dV_j}{\omega},$$

$$a_{61} = a_{62} = 0, \quad a_{6l} = -(d_{12} + d_{13})k_i\frac{\xi_R}{\omega}\frac{dV_i}{\omega}, \quad a_{6k} = l_j\left(d_{13}\frac{dV_{j'}^2}{\omega^2} - d_{12}\frac{\xi_R^2}{\omega^2}\right),$$

$$a_{71} = -\iota\frac{d\mathrm{V}_{\alpha'}}{\omega}, \quad a_{72} = \iota\frac{\xi_R}{\omega}, \quad a_{7l} = -\iota\frac{dV_i}{\omega}, \quad a_{7k} = -\iota\frac{\xi_R}{\omega},$$

$$a_{81} = \iota\frac{\xi_R}{\omega}, \quad a_{82} = \iota\frac{d\mathrm{V}_{\beta'}}{\omega}, \quad a_{8l} = -\iota\frac{\xi_R}{\omega}, \quad a_{8k} = \iota\frac{dV_j}{\omega},$$

$$a_{91} = a_{92} = 0, \quad a_{9l} = \iota n_i\frac{dV_i}{\omega}, \quad a_{9k} = 0$$

$$(i = 1, 2, 3, 4, l = 3, 4, 5, 6,\ k = 7, 8, 9 \text{ and } j = 5, 6, 7)$$

$$d_1 = \frac{\rho c_1^2}{\nu T_0}, \quad d_2 = \frac{\lambda}{\nu T_0}, \quad d_3 = \frac{\lambda_0}{\nu T_0} \quad d_4 = \frac{\mu}{\nu T_0}, \; d_5 = \frac{K}{\nu T_0}, \quad d_6 = \frac{\gamma}{L^2 \nu T_0},$$
$$d_7 = \frac{b_0}{L^2 \nu T_0}, \quad d_8 = \frac{\alpha_0}{L^2 \nu T_0}, \quad d_{10} = \frac{k_4}{L^3 c_1 \nu T_0}, \quad d_{11} = \frac{k_5 + k_6}{L^3 c_1 \nu T_0}, \quad d_{12} = \frac{k_5}{L^3 c_1 \nu T_0},$$
$$d_{13} = \frac{k_6}{L^3 c_1 \nu T_0}, \quad \overline{d_1} = \frac{\lambda^e + 2\mu^e}{\nu T_0}, \quad \overline{d_2} = \frac{\lambda^e}{\nu T_0}, \quad \overline{d_3} = \frac{\mu^e}{\nu T_0}$$

13 Appendix V

$$a_{11} = \left[\overline{d_1} \frac{dV_{\alpha'}^2}{\omega^2} + \overline{d_2} \frac{\xi_R^2}{\omega^2} \right], \quad a_{12} = -\left(\overline{d_1} - \overline{d_2}\right) \frac{\xi_R}{\omega} \frac{dV_{\beta'}}{\omega},$$
$$a_{1l} = -d_1 \frac{dV_{i'}^2}{\omega^2} - d_2 \frac{\xi_R^2}{\omega^2} + d_3 \frac{m_i}{\omega^2}, \quad a_{1k} = -\left(d_1 - d_2\right) \frac{\xi_R}{\omega} \frac{dV_j}{\omega},$$
$$a_{21} = 2\overline{d_3} \frac{\xi_R}{\omega} \frac{dV_{\alpha'}}{\omega}, \quad a_{22} = \overline{d_3} \left(\frac{dV_{\beta'}^2}{\omega^2} - \frac{\xi_R^2}{\omega^2} \right), \quad a_{2l} = 2d_4 \frac{dV_i}{\omega} \frac{\xi_R}{\omega}, \quad a_{2k} = -d_4 \frac{dV_{j'}^2}{\omega^2} + d_4 \frac{\xi_R^2}{\omega^2},$$
$$a_{31} = a_{32} = 0, \quad a_{3l} = \iota d_8 m_i \frac{d\mathrm{V}_i}{\omega}, \quad a_{3k} = -\iota d_9 g_j \frac{\xi_R}{\omega},$$
$$a_{41} = a_{42} = 0, \quad a_{4l} = \left[-d_{10} \frac{\xi_R^2}{\omega^2} - \left(d_{10} + d_{11}\right) \frac{dV_{i'}^2}{\omega^2} \right] k_i, \quad a_{4k} = -d_{11} l_j \frac{\xi_R}{\omega} \frac{dV_j}{\omega},$$
$$a_{51} = a_{52} = 0, \quad a_{5i} = -\left(d_{12} + d_{13}\right) k_i \frac{\xi_R}{\omega} \frac{dV_i}{\omega}, \quad a_{5k} = l_j \left(d_{13} \frac{dV_{j'}^2}{\omega^2} - d_{12} \frac{\xi_R^2}{\omega^2} \right),$$
$$a_{61} = -\iota \frac{d\mathrm{V}_{\alpha'}}{\omega}, \quad a_{62} = \iota \frac{\xi_R}{\omega}, \quad a_{6l} = -\iota \frac{dV_i}{\omega}, \quad a_{6k} = -\iota \frac{\xi_R}{\omega}, \quad a_{71} = \iota \frac{\xi_R}{\omega}, \quad a_{72} = \iota \frac{d\mathrm{V}_{\beta'}}{\omega},$$
$$a_{7l} = -\iota \frac{\xi_R}{\omega}, \quad a_{7k} = \iota \frac{dV_j}{\omega}, \quad a_{81} = a_{82} = 0, \quad a_{8l} = \iota n_i \frac{dV_i}{\omega}, \quad a_{8k} = 0$$
$$(i = 1, 2, 3, 4, \; l = 3, 4, 5, 6, \quad k = 7, 8 \text{ and } j = 5, 6, 7)$$

References

1. Eringen, A.C.: Linear theory of micropolar elasticity. J. Math. Mech. **15**, 909–923 (1966a)
2. Eringen, A.C.: Theory of micropolar elasticity. In: Liebowitz, H. (ed.) Fracture vol .II, Chap. 7, pp. 621–729. Academic Press, New York (1968a)
3. Eringen, A.C., Demiray, H.: A two dimensional lattice model of composites reinforced with orthogonal fibres. Appl. Eng. Sci. **3**, 295–309 (1975)
4. Eringen, A.C.: Micropolar theory of liquid crystals. In: Johnson, J.F., Porter, R.S. (eds.) Liquid Crystal and Ordered Fluids **3**, 443–473, Plenum, New York (1978)
5. Eringen, A.C.: Micropolar elastic solids with stretch. In: Prof. Dr. Mustafa Inan Anisiana, Ari Kitabevi Matbassi **24**, 1–18 (1971)
6. Eringen, A.C.: Theory of thermo-microstretch elastic solids. Int. J. Eng. Sci. **28**, 1291–1301 (1990)
7. Eringen, A.C.: Mechanics of micromorphic materials. In: Gortler, H. (ed.) Proceedings of the 2nd International Congress of Applied Mechanics, pp. 131–138. Springer, Berlin (1966b)
8. Eringen, A.C.: Mechanics of micromorphic continua. In: Kroner, E. (ed.) Mechanics of Generalized Continua, IUTAM Symposium, Freudenstadt-Stuttgart, pp. 18-35. Springer, Berlin (1968b)
9. Singh, B.: Reflection of plane waves from free surface of a microstretch elastic solid. Proc. Sect. A Earth Planet. Sci. **111**, 29–37 (2002)
10. Singh, B., Kumar, R.: Wave propagation in a generalized thermo-microstretch elastic solid. Int. J. Eng. Sci. **36**, 891–912 (2003)
11. Ciarletta, M., Scalia, A.: Some Results in Linear Theory of Thermomicrostretch Elastic Solids. Meccanica **39**, 191–206 (2004)
12. Iesan, D., Quintanilla, R.: Thermal stresses in microstretch elastic plates. Int. J. Eng. Sci. **43**, 885–907 (2005)
13. Tomar, S.K., Khurana, A.: Reflection and transmission of elastic waves from a plane interface between two thermo-microstretch solid half-spaces. Int. J. Appl. Math. Mech. **5**, 48–68 (2009)

14. Abbas, I.A., Othman, M.I.A.: Plane Waves in generalized thermo-microstretch elastic solid with thermal relaxation using finite element method. Int. J. Thermophys. **33**, 2407–2423 (2012)
15. Kumar, S., Sharma, J.N., Sharma, Y.D.: Generalized thermoelastic waves in microstretch plates loaded with fluid of varying temperature. Int. J. Appl. Mech. **3**, 563–586 (2011)
16. Kumar, R., Partap, G.: Elastodynamic behavior of waves in thermo-microstretch elastic plate bordered with layers of inviscid liquid. Int. J. Thermophys. **30**, 2122–2143 (2009a)
17. Kumar, R., Partap, G.: Wave propagation in microstretch thermoelastic plate bordered with layers of inviscid liquid. Multidiscip. Model. Mater. Struct. **5**, 171–184 (2009b)
18. Kumar, R., Partap, G.: Analysis of free vibrations for Rayleigh—Lamb waves in a microstretch thermoelastic plate with two relaxation times. Thai J. Math. **8**, 73–102 (2010)
19. Kumar, R. Rupender: Reflection at free surface of magneto-thermo-microstretch elastic solid. Bull. Pol. Acad. Sci. **56**, 263–271 (2008)
20. Kumar, R. Rupender: Propagation of plane waves at imperfect boundary of elastic and elctro-microstretch generalized thermoelastic solids. Appl. Math. Mech. **30**, 1445–1454 (2012)
21. Kumar, R., Kansal, T.: Fundamental solution in the theory of thermomicrostretch elastic diffusive solids. ISRN Appl. Math. **2011**, 1–15 (2011)
22. Marin, M.: A partition of energy in thermoelasticity of microstretch bodies. Nonlinear Anal.: Real World Appl. **11**, 2436–2447 (2010a)
23. Marin, M.: Lagrange identity method for microstretch thermoelastic materials. J. Math. Anal. Appl. **363**, 275–286 (2010b)
24. Othman, M.I.A, Lofty, K.H.: On the plane waves of generalized thermomicrostretch elastic half space under three theories. Int. Commun. Heat Mass Transf. **37**, 192–200 (2010)
25. Othman, M.I.A., Lofty, K.H.: Effect of rotation on plane waves in generalized thermo-microstretch elastic solid with one relaxation time. Multidiscip. Model. Mater. Struct. **7**, 43–62 (2011)
26. Othman, M.I.A., Lofty, K.H., Farouk, R.M.: Generalized thermo-microstretch elastic medium with temperature dependent properties for different theories. Eng. Anal. Boundary Elem. **43**, 229–237 (2010)
27. Passarella, F., Tibullo, V.: Some results in linear theory of thermoelasticity backward in time for microstretch materials. J. Therm. Stress. **33**, 559–576 (2010)
28. Passarella, F., Tibullo, V., Zampoli, V.: On microstretch thermoviscoelastic composite materials. Eur. J. Mech. A Solids **37**, 294–303 (2013)
29. Shaw, S., Mukhopadhayay, B.: Electromagnetic effects on Rayleigh surface wave propagation in a homogeneous isotropic thermo-microstretch elastic half-space. J. Eng. Phys. Thermophys. **85**, 229–238 (2012)
30. Grot, R.A.: Thermodynamics of a continuum with microstructure. Int. J. Eng. Sci. **7**, 801–814 (1969)
31. Riha, P.: On the microcontinuum model of heat conduction in materials with inner structure. Int. J. Eng. Sci. **14**, 529–535 (1976)
32. Iesan, D., Quintanilla, R.: On a theory of thermoelasticity with microtemperatures. J. Therm. Stress. **23**, 199–215 (2000)
33. Iesan, D.: On a theory of micromorphic elastic solids with microtemperatures. J. Therm. Stress. **24**, 737–752 (2001)
34. Iesan, D., Quintanilla, R.: On thermoelastic bodies with inner structure and microtemperatures. J. Math. Anal. Appl. **354**, 12–23 (2009)
35. Casas, P.S., Quintanilla, R.: Exponential stability in thermoelasticity with microtemperatures. Int. J. Eng. Sci. **43**, 33–47 (2005)
36. Scalia, A., Svanadze, M.: On the representation of solutions of the theory of thermoelasticity with microtemperatures. J. Therm. Stress. **29**, 849–863 (2006)
37. Iesan, D.: Thermoelasticity of bodies with microstructure and microtemperatures. Int. J. Solids Struct. **43**, 3414–3427 (2006)
38. Aouadi, M.: Some theorems in the isotropic theory of microstretch thermoelasticity with microtemperatures. J. Therm. Stress. **31**, 649–662 (2008)
39. Scalia, A., Svanadze, M., Tracinà, R.: Basic theorems in the equilibrium theory of thermoelasticity with microtemperatures. J. Therm. Stress. pp. 721–753 (2010)
40. Quintanilla, R.: On growth and continous dependence in thermoelasticity with microtemperatures. J. Therm. Stress. **34**, 911–922 (2011)
41. Steeb, H., Singh, J., Tomar, S.K.: Time harmonic waves in thermoelastic material with microtemperatures. Mech. Res. Commun. **48**, 8–18 (2013)
42. Chirita, S., Ciarletta, M., D'Apice, C.: On the theory of thermoelasticity with microtemperatures. J. Math. Anal. Appl. **397**, 349–361 (2013)
43. Iesan, D.: Thermoelasticity of bodies with microstructure and microtemperatures. Int. J. Solids Struct. **44**, 8648–8662 (2007)
44. Bullen, K.E.: An Introduction of the Theory of Seismology. Cambridge University Press, Cambridge (1963)
45. Borcherdt, R.D.: Reflection-refraction of general P and type-I S waves in elastic and an elastic solids. Geophys. J. R. Astron. Soc. **70**, 621–638 (1982)
46. Eringen, A.C.: Plane waves in non local micropolar elasticity. Int. J. Eng. Sci. **22**, 1113–1121 (1984)
47. Dhaliwal, R.S., Singh, A.: Dynamic Coupled Thermoelasticity. Hindustan Publication Corporation, New Delhi (1980)